Linear and nonlinear modes in nonrelativistic electron-positron plasmas

G. P. Zank
Bartol Research Institute, University of Delaware, Newark, Delaware 19716

R. G. Greaves
Physics Department, University of California, San Diego, La Jolla, California 92093
(Received 4 August 1994; revised manuscript received 9 February 1995)

A comprehensive two-fluid model is developed for collective modes in a nonrelativistic electron-positron plasma. Longitudinal and transverse electrostatic and electromagnetic modes, both in the presence and absence of a magnetic field, are studied. Wave properties are discussed in terms of dispersion relations, wave normal surfaces, and Clemmow-Mullaly-Allis diagrams. The results are extended to include the two-stream instability and ion acoustic solitary waves. For the two-stream instability, a similar result is found as in the electron-ion plasma. For ion acoustic solitary waves, only subsonic solutions are found to exist. Furthermore, their width is proportional to their amplitude, unlike the electron-ion plasma case, where the speed is proportional to the amplitude.

PACS number(s): 52.25.−b, 52.35.Hr, 52.35.Qz, 52.35.Sb

I. INTRODUCTION

Recent progress in the production of pure positron plasmas [1–3] now makes it possible to consider performing laboratory experiments on electron-positron (hereinafter referred to as e^+e^-) plasmas. Indeed, e^+e^- plasmas represent the larger class of equal-mass plasmas, a class of plasmas that may offer plasma physical properties quite different from those of conventional ion-electron plasmas. In the analysis of conventional plasmas, the ratio of electron mass m_e to ion mass m_i is exploited to great effect leading one to distinguish, for example, between high (electron dominated) and low (ion dominated) frequency motions. Conversely, with both constituent species possessing the same absolute charge to mass ratio, important symmetries manifest themselves, leading to considerable simplifications in the mathematical description of equal-mass plasmas. Theoretical interest in e^+e^- plasmas has focused largely on the relativistic regime, since such plasmas are thought to be produced naturally under certain astrophysical conditions [4–9]. However, nonrelativistic plasmas are also of astrophysical interest: as has been widely noted, electron-positron plasmas radiate very effectively by cyclotron emission and must, therefore, cool eventually. Despite this, the nonrelativistic regime has received less theoretical attention. Tsytovich and Wharton [10] presented preliminary theoretical results as well as an idea for a magnetic mirror device in which to perform e^+e^- experiments. More recently, Iwamoto [11] presented a kinetic theory treatment of waves in an e^+e^- system, while Stewart and Laing [12] used a multifluid description to study certain aspects of wave propagation. Recent studies have also treated some nonlinear phenomena [13] and transport issues [14].

Clearly, a careful and comprehensive analysis of the elementary plasma properties of an e^+e^- system is desirable, both to extend and complement existing theory as well as to provide guidelines for planned experiments. In this paper, we investigate a simple multifluid description of an e^+e^- plasma in a manner that reveals clearly the natural symmetries inherent in the system.

A number of experimental approaches have been proposed for studying e^+e^- plasmas in the laboratory and several of these are now being actively pursued. Early experiments trapped relativistic positrons directly into a magnetic mirror from radioactive neon gas [15,16], although the positron density was too low for positron plasma studies. Tsytovich and Wharton [10] proposed trapping positrons in a magnetic mirror from a LINAC source. More recently, Boehmer [17] has employed cyclotron heating to trap moderated positrons from a radioactive source and to heat the trapped positrons to relativistic energies [17]. Another approach that is currently being tested experimentally is to trap positrons from a LINAC source into a Penning trap by a gate-switching technique [18,19]. Electron-positron plasma experiments using the cold, trapped positrons could then be accomplished in a transient fashion using multiple electrostatic wells. Yet another approach to confining both electrons and positrons simultaneously is to employ the Paul trap [20]. This technique has already been applied to ion plasmas with opposite signs of charge but there have been no experimental demonstrations for positrons and electrons where rf heating of the confined plasmas is a potentially serious obstacle.

The most successful experimental approach to obtaining positron plasmas is by scattering from a buffer gas into a Penning trap. Up to 10^8 positrons can now be stored at densities of more than 2×10^6 cm^{-3}. These clouds of positrons constitute robust plasmas in which collective plasma modes can be excited easily, and electron-positron plasma experiments are now being pursued by injecting a low-energy electron beam into the positrons [21].

In electron-positron plasmas, pair annihilation can take place. This process is analogous to recombina-

 ©1995 The American Physical Society

tion in electron-ion plasmas. A requirement for collective plasma effects to play a role is that the annihilation time scale should be much longer than the time scale for plasma effects, which is typically the inverse of the plasma frequency. Pair annihilation can take place by a number of processes, the most important of which are annihilation in two-body collisions and annihilation via positronium atom formation. In addition, at very high densities, induced annihilation has been predicted, with possible application as a γ-ray laser. Positron annihilation in e^+e^- plasmas has been treated in detail by many authors (see, e.g., Refs. [22] and [23]) and so only a brief resume is given here. At low energies, positronium atom formation by radiative recombination dominates the loss process. The singlet state of the positronium atom decays in about 10^{-10} s while the triplet state decays in about 10^{-7} s. At 300 K the recombination rate is about 10^{-11} cm^3 s^{-1}, so that for a realistic plasma density of 10^{10} cm^{-3}, the annihilation time from positronium atom formation would be about 10 s while the direct annihilation time would about 100 s. Both of these time scales are many orders of magnitude larger than the plasma period of 10^{-9} s so that long-time-scale plasma physics experiments should be possible.

For energies above 100 eV, direct annihilation dominates the loss process. For example, for 10-keV positrons, the direct annihilation rate is about 10^{-14} cm^3 s^{-1}, i.e., even lower than at low energies, so that once again, long-time-scale experiments should be possible

This paper is structured as follows. Section II deals with the multifluid equations. In Sec. III, the wave properties of the plasma are discussed in terms of dispersion relations, wave normal surfaces and Clemmow-Mullaly-Allis (CMA) diagrams. A beam-plasma system is discussed in Sec. IV, while results for stationary solitary wave structures are presented in Sec. V. The paper is summarized in Sec. VI.

II. MULTIFLUID EQUATIONS

The multifluid equations appropriate to an e^+e^- plasma consist of the usual continuity and momentum equations for each species, supplemented by Maxwell's equations. We assume that the pressure p_j ($j = e, p$) is isotropic and satisfies $p_j = \gamma\kappa T_j n_j$ where $n_j \equiv$ number density of species j, γ is the ratio of specific heats, κ is Boltzmann's constant, and T_j is the species temperature.

Since it is easier to transfer momentum between particles of equal mass than between particles of unequal mass (momentum transfer per collision is proportional to m/M when $m < M$), the equilibration time scales for electrons and positrons are equal. Consequently, both species will reach a self-equilibrium together, and a global equilibrium will result at the same time. Hence, we may take the temperatures of both species to be equal—the first of the important simplifications arising from symmetries associated with an e^+e^- plasma.

The model equations are, therefore,

$$\frac{\partial n_j}{\partial t} + \nabla \cdot (n_j \mathbf{u}_j) = 0, \tag{1}$$

$$mn_j \left(\frac{\partial \mathbf{u}_j}{\partial t} + \mathbf{u}_j \cdot \nabla \mathbf{u}_j \right) = -\nabla p_j + q_j n_j \left(\mathbf{E} + \frac{1}{c} u_j \times \mathrm{B} \right), \tag{2}$$

$$\nabla \cdot \mathrm{E} = 4\pi e \left(n_p - n_e \right), \tag{3}$$

$$\nabla \times \mathbf{E} = -\frac{1}{c}\frac{\partial B}{\partial t}, \tag{4}$$

$$\nabla \times \mathbf{B} = \frac{4\pi}{c}\mathbf{J} + \frac{1}{c}\frac{\partial \mathbf{E}}{\partial t}, \tag{5}$$

$$\nabla \cdot \mathbf{B} = 0, \qquad \mathbf{J} = e \left(n_p \mathbf{u}_p - n_e \mathbf{u}_e \right), \tag{6}$$

where q_j denotes the charge (either e or $-e$, $j = e, p$), $\mathbf{u}_j$ the fluid velocity, c the speed of light, m the electron mass, and $\mathbf{E}$ and $\mathbf{B}$ the electric and magnetic fields, respectively.

III. LINEAR WAVE PROPAGATION

By linearizing Eqs. (1)–(6) about an equilibrium state, we can investigate the propagation of small amplitude waves in an e^+e^- plasma. The results presented here complement and extend those presented by Iwamoto [11] and Stewart and Laing [12].

A. Electrostatic modes with $B = 0$

In the absence of an applied magnetic field and magnetic fluctuations, and linearizing about a homogeneous unbounded plasma (using $n_j \to N_j + n_j$, $\mathbf{u}_j \to \mathbf{0} + \mathbf{u}_j$, $N_e = N_p = N$ and $T_e = T_p = T$), we can reduce Eqs. (1)–(6) to the coupled linear wave equations

$$\left(\frac{\partial^2}{\partial t^2} - C_s^2 \nabla^2 \right) (n_e + n_p) = 0, \tag{7}$$

$$\left(\frac{\partial^2}{\partial t^2} - C_s^2 \nabla^2 + 2\omega_p^2 \right) (n_e - n_p) = 0. \tag{8}$$

The acoustic speed $C_s^2 \equiv \gamma\kappa T/m$ and plasma frequency $\omega_p^2 \equiv 4\pi e^2 N/m$ have been introduced. Equation (7), for the sum of the electron and positron fluctuations, describes the propagation of acoustic waves. The difference $n_e - n_p$ in density fluctuations propagates as a Langmuir wave and the combined contribution from both electrons and positrons yields the fundamental plasma frequency for the system as $\sqrt{2}\omega_p$. For perturbations $\propto \exp[i(\omega t - \mathbf{k} \cdot \mathbf{x})]$, the dispersion relations associated with (7) and (8) are simply

$$\omega^2 = C_s^2 k^2, \tag{9}$$

$$\omega^2 = C_s^2 k^2 + 2\omega_p^2, \tag{10}$$

plots of which are illustrated in Fig. 1. These modes

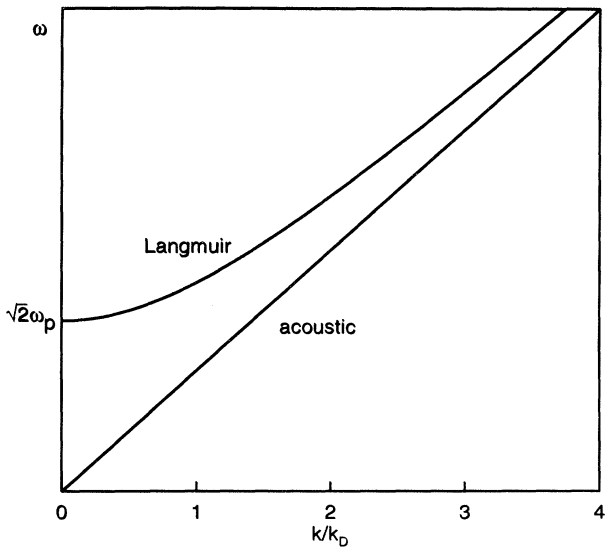

FIG. 1. Dispersion relation for electrostatic waves with $B = 0$, showing the acoustic and Langmuir branches. In practice, the acoustic branch is heavily damped.

are simply the acoustic and Langmuir waves, respectively. Tsytovich and Wharton have pointed out that the acoustic wave is heavily damped in e^+e^- plasmas having $T_e = T_p$. This phenomenon arises from Landau damping, which is maximized for waves traveling at speeds where the slope of the distribution function is maximum, i.e., at $\omega/k = C_s$.

B. Electrostatic modes with $B \neq 0$

Consider a nonzero applied magnetic field $\mathbf{B}_0 \neq \mathbf{0}$ but for which magnetic fluctuations $\delta\mathbf{B} = \mathbf{0}$. Without loss of generality, suppose $\mathbf{B}_0 = B_0\hat{\mathbf{z}}$ and introduce the gyrofrequency $\Omega_p \equiv eB_0/mc$. After linearizing (1)–(6), we derive the coupled wave equations

$$\left[\frac{\partial^2}{\partial t^2}\left(\frac{\partial^2}{\partial t^2} - C_s^2\nabla^2 + \Omega_p^2\right) - C_s^2\Omega_p^2\frac{\partial^2}{\partial z^2}\right](n_e + n_p) = 0, \tag{11}$$

$$\left[\left(\frac{\partial^2}{\partial t^2} + 2\omega_p^2\right)\left(\frac{\partial^2}{\partial t^2} - C_s^2\nabla^2 + 2\omega_p^2 + \Omega_p^2\right) - C_s^2\Omega_p^2\frac{\partial^2}{\partial z^2}\right](n_e - n_p) = 0, \tag{12}$$

where, once again, the symmetries inherent in an equal-mass plasma lead to considerable simplifications in the analysis and yield the above factorization. On using the convention $\hat{\mathbf{k}} \equiv (0, \sin\theta, \cos\theta)$ together with $n_j \propto \exp[i(\omega t - \mathbf{k}\cdot\mathbf{x})]$, we obtain the dispersion relations governing magnetostatic modes in an e^+e^- plasma,

$$\omega^2\left(\omega^2 - C_s^2k^2 - \Omega_p^2\right) + C_s^2\Omega_p^2k^2\cos^2\theta = 0, \tag{13}$$

$$\left(\omega^2 - 2\omega_p^2\right)\left(\omega^2 - C_s^2k^2 - \Omega_h^2\right) + C_s^2\Omega_p^2k^2\cos^2\theta = 0, \tag{14}$$

where we have introduced the hybrid frequency $\Omega_h^2 \equiv 2\omega_p^2 + \Omega_p^2$.

The dispersion relation (13) is plotted in Fig. 2(a) for various values of θ from 0 to $\pi/2$. The modes shown correspond to acoustic and cyclotron waves in an electron-ion plasma. Similarly, Eq. (14) is plotted in Fig. 2(b), which shows modes that correspond to Langmuir and (upper) hybrid waves. It is instructive to tabulate (Table I) the various electrostatic wave modes for propagation parallel and perpendicular to the applied magnetic field. For comparison, we also list the nomenclature used for the equivalent mode in an ion-electron plasma. Not surprisingly, there are no angular limitations on the propagation of cyclotron modes, unlike the lower hybrid modes in an ion-electron plasma—a conclusion similar to that obtained in Ref. [10].

By introducing the refractive index vector $\mathbf{n} \equiv C_s\mathbf{k}/\omega$, we rewrite (13) and (14) as

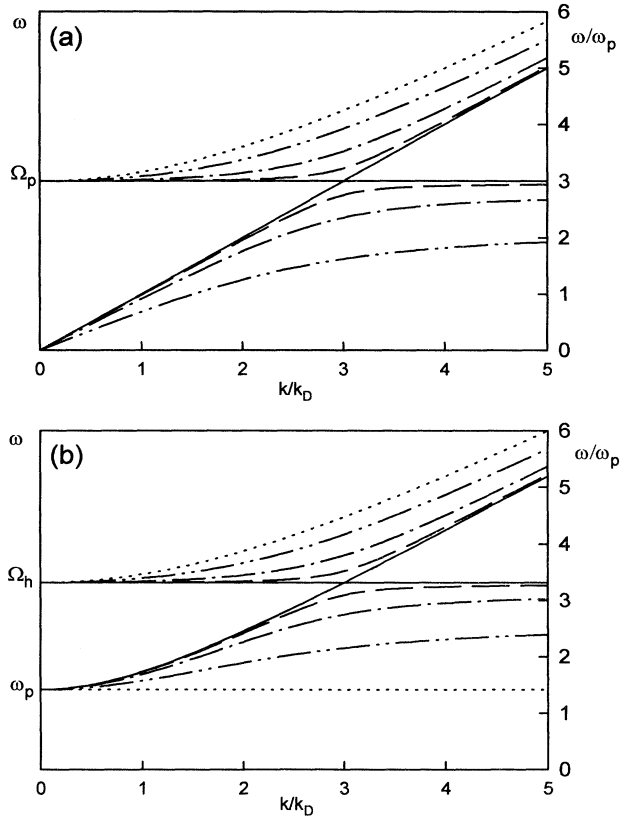

FIG. 2. Dispersion relation of electrostatic waves with $B \neq 0$ for various angles of propagation showing, (a) the acoustic and cyclotron branches and (b) the upper hybrid and Langmuir branches. Solid lines, $\theta = 0$; dashed lines, $\theta = \pi/20$; chain curve, $\theta = \pi/8$; double chain curve $\theta = \pi/4$; dotted line, $\theta = \pi/2$.

TABLE I. Summary of electrostatic modes.

$\theta = 0$		$\theta = \pi/2$	
Dispersion relation	Identification	Dispersion relation	Identification
$\omega^2 = C_s^2 k^2$	acoustic wave	$\omega = 0$	nonpropagating
$\omega^2 = \Omega_p^2$	cyclotron oscillation	$\omega^2 = C_s^2 k^2 + \Omega_p^2$	cyclotron waves
$\omega^2 = 2\omega_p^2 + \Omega_p^2$	upper hybrid oscillation	$\omega^2 = C_s^2 k^2 + 2\omega_p^2 + \Omega_p^2$	upper hybrid wave
$\omega^2 = C_s^2 k^2 + 2\omega_p^2$	Langmuir waves	$\omega^2 = 2\omega_p^2$	Langmuir oscillation

$$n^2 = \frac{\omega^2 - \Omega_p^2}{\omega^2 - \Omega_p^2 \cos^2\theta} = \frac{1 - Y^2}{1 - Y^2\cos^2\theta}, \tag{15}$$

$$n^2 = \frac{\left(1 - 2\omega_p^2/\omega^2\right)\left(1 - 2\omega_p^2/\omega^2 - \Omega_p^2/\omega^2\right)}{1 - 2\omega_p^2/\omega^2 - \Omega_p^2/\omega^2\cos^2\theta} = \frac{(1-X)(1-X-Y^2)}{1 - X - Y^2\cos^2\theta}, \tag{16}$$

where, following Clemmow and Dougherty [24], $Y = \Omega_p/\omega$ and $X = 2\omega_p^2/\omega^2$. The resonances are sensitive to the magnetic field and are found at $\omega = \Omega_p \cos\theta$ and $\omega = (2\omega_p^2 + \Omega_p^2\cos^2\theta)^{1/2}$ while cutoff frequencies are located at $\omega = \sqrt{2}\omega_p$, Ω_p, and Ω_h. A convenient characterization of the general wave properties of the magnetostatic modes in an e^+e^- plasma is to plot $n^2(\omega)$—illustrated for $\omega_p = \Omega_p/2$ in Fig. 3. The low-frequency curve in the upper left corner of Fig. 3 corresponds to the acoustic mode, which disappears as $\theta \to \pi/2$.

The Clemmow-Mullaly-Allis, or CMA, diagram is a useful tool for classifying waves in a cold plasma. From (15) and (16), the two free parameters X and Y can be used to collate the different topologies of the refractive index surface. For the dispersion relation (13), one can easily sketch the refractive index surface $n(\theta)$ for the two cases $0 < Y < 1$ [Fig. 4(a)] and $Y > 1/\cos\theta$ [Fig. 4(b)]. The usefulness of the refractive index curves is that a normal to a point P on the surface represents the direction of energy flow for a plane wave propagating in the direction OP. The critical angle $\theta_c \equiv \cos^{-1} Y^{-1}$, depicted in Fig. 4(b), defines the asymptote to the hyperbolic refractive index surface. The CMA diagram corresponding to the modes described by (13) is illustrated in Fig. 4(c). Three distinct regions are apparent: (i) $Y < 1$ or $\omega > \Omega_p$ (cyclotron), (ii) an evanescent region $1 < Y < 1/\cos\theta$ in which wave propagation is forbidden, and (iii) the low-frequency band $Y > 1/\cos\theta$, i.e., $\omega < \Omega_p \cos\theta$ (acoustic mode).

Turning now to the dispersion relation (14), similar refractive index curves are obtained [Figs. 5(a) and (b)] although now with a plasma frequency dependence. The appropriate CMA diagram is illustrated in Fig. 5(c), and

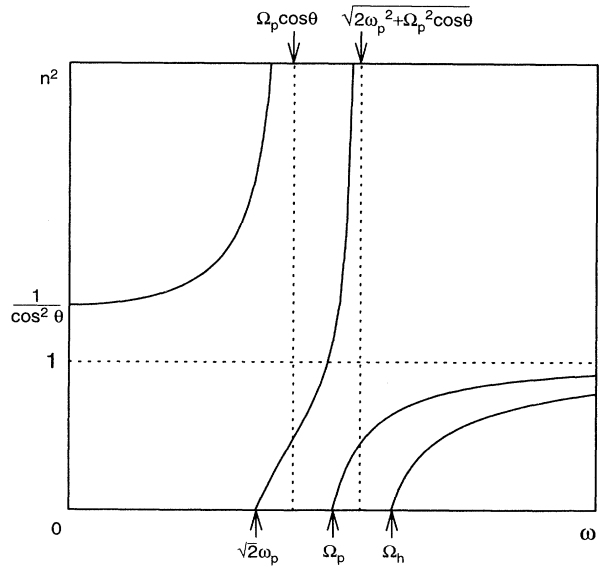

FIG. 3. Refractive index curves for electrostatic waves with $B \neq 0$.

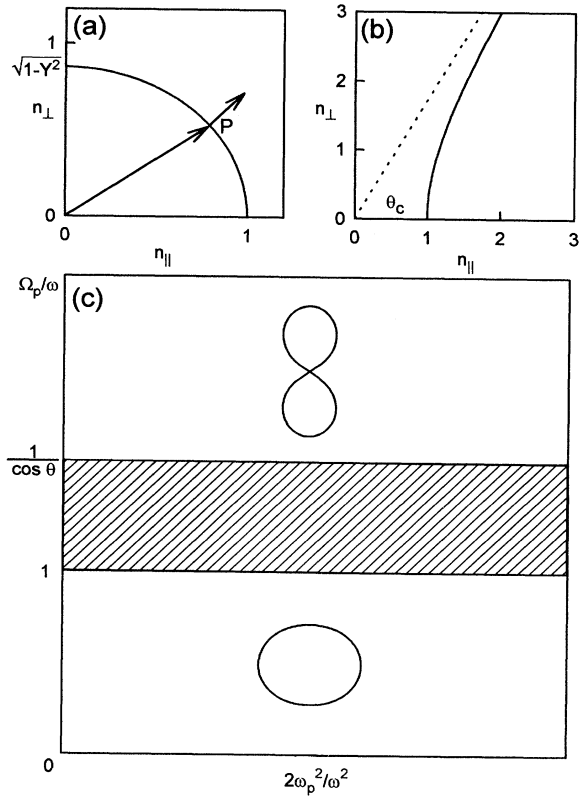

FIG. 4. Properties of electrostatic waves with $B \neq 0$. Wave normal curves for (a) the acoustic and (b) the cyclotron branches of the dispersion relation. (c) CMA diagram showing the stop band where waves are evanescent (hatched). The insets are polar plots of the inverse of the wave normal curves shown in (a) and (b).

we see that $X < 1$ is necessary for wave propagation. The curved boundaries of Fig. 5 are defined by the cutoff at $X + Y^2 = 1$ and the resonance $X + Y^2 \cos^2\theta = 1$. Waves in the region bounded by these curves are evanescent, hence wave propagation is restricted to the regions (i) $X < 1$, $X + Y^2 < 1$, i.e., $\Omega_h^2 < \omega^2$, and (ii) $X < 1$, $X + Y^2\cos^2\theta > 1$ or $2\omega_p^2 < \omega^2$, $2\omega_p^2 + \Omega_p^2\cos^2\theta > \omega^2$.

C. Electromagnetic modes

Let us now consider both an applied magnetic field $\mathbf{B}_0 = B_0\hat{\mathbf{z}}$ and magnetic field fluctuations. For reference, the full set of linearized equations is written down, where $\mathbf{B} = \mathbf{B}_0 + \mathbf{B}$,

$$\frac{\partial n_j}{\partial t} + N\nabla\cdot\mathbf{u}_j = 0,$$

$$mN\frac{\partial \mathbf{u}_j}{\partial t} + \gamma\kappa T\nabla n_j = qN\left(\mathbf{E} + \frac{1}{c}\mathbf{u}_j\times\mathbf{B}_0\right),$$

$$\nabla\cdot\mathbf{E} = 4\pi e\left(n_p - n_e\right),$$

$$\nabla\times\mathbf{E} = -\frac{1}{c}\frac{\partial\mathbf{B}}{\partial t},$$

$$\nabla\times\mathbf{B} = \frac{4\pi}{c}eN\left(\mathbf{u}_p - \mathbf{u}_e\right) + \frac{1}{c}\frac{\partial\mathbf{E}}{\partial t}.$$

Some straightforward algebra then yields two coupled linear wave equations in the electron and positron densities,

$$\left[\frac{\partial^2}{\partial t^2}\left(\frac{\partial^2}{\partial t^2} - c^2\nabla^2 + 2\omega_p^2\right)\left(\frac{\partial^2}{\partial t^2} - C_s^2\right) + \Omega_p^2\left(\frac{\partial^2}{\partial t^2} - C_s^2\frac{\partial^2}{\partial z^2}\right)\left(\frac{\partial^2}{\partial t^2} - c^2\nabla^2\right)\right]\left(n_e + n_p\right) = 0, \tag{17}$$

$$\left[\frac{\partial^2}{\partial t^2}\left(\frac{\partial^2}{\partial t^2} - c^2 + 2\omega_p^2\right)\left(\frac{\partial^2}{\partial t^2} - C_s^2\nabla^2 + 2\omega_p^2 + \Omega_p^2\right) - \Omega_p^2C_s^2\frac{\partial^2}{\partial z^2}\left(\frac{\partial^2}{\partial t^2} - c^2\nabla^2 + 2\omega_p^2\frac{c^2}{C_s^2}\right)\right]\left(n_e - n_p\right) = 0. \tag{18}$$

The electromagnetic e^+e^- dispersion relation, therefore, admits the bicubic (in ω^2) factorization

$$\omega^2\left(\omega^2 - c^2k^2 - 2\omega_p^2\right)\left(\omega^2 - C_s^2k^2\right)$$

$$-\Omega_p^2\left(\omega^2 - C_s^2k^2\cos^2\theta\right)\left(\omega^2 - c^2k^2\right) = 0, \tag{19}$$

$$\omega^2\left(\omega^2 - c^2k^2 - 2\omega_p^2\right)\left(\omega^2 - C_s^2k^2 - \Omega_h^2\right)$$

$$+\Omega_p^2C_s^2k^2\cos^2\theta\left(\omega^2 - c^2k^2 - 2\omega_p^2c^2/C_s^2\right) = 0. \tag{20}$$

For the purpose of identifying the respective modes, it is useful to factorize the bicubic dispersion relations (19) and (20) for the special cases of wave propagation parallel and perpendicular to the applied magnetic field.

Consider first Eq. (19). For perpendicular propagation, this equation reduces to the biquadratic

$$\omega^2[\omega^4 - \left(c^2k^2 + C_s^2k^2 + \Omega_h^2\right)\omega^2$$

$$+C_s^2k^2\left(c^2k^2 + 2\omega_p^2\right) + \Omega_p^2c^2k^2] = 0,$$

or

$$\omega^2\left(\omega^2 - \omega_{\perp-}^2\right)\left(\omega^2 - \omega_{\perp+}^2\right) = 0, \tag{21}$$

where we have introduced

$$2\omega_{\perp\pm}^2 = (c^2 + C_s^2)k^2 + \Omega_h^2 \pm\sqrt{(c^2k^2 + C_s^2k^2 + \Omega_h^2)^2 + 8\omega_p^2\Omega_p^2}. \tag{22}$$

Observe that for $k = 0$, $\omega_{\perp\pm}^2 = 0, \Omega_h^2$ and, as $k\to\infty$, the $\omega_{\perp\pm}$ are asymptotic to the lines ck and C_sk. Conse-

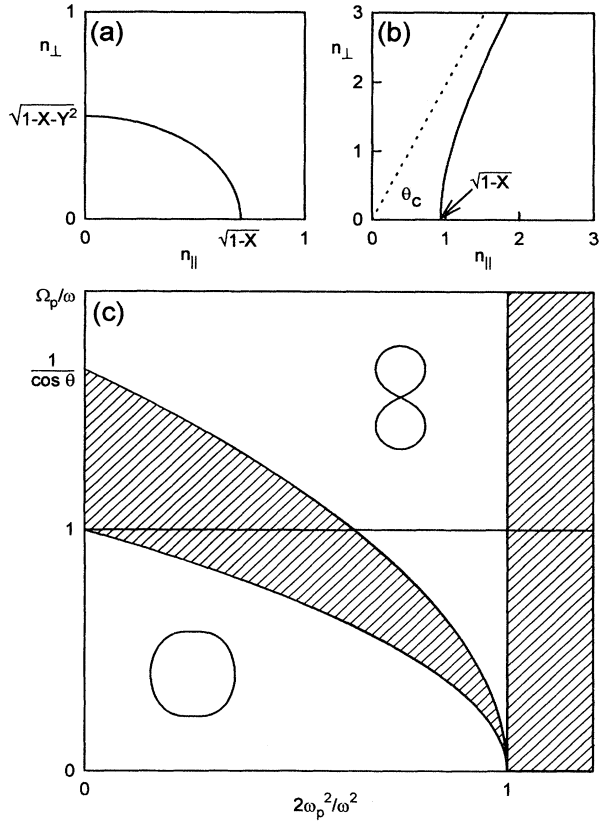

FIG. 5. Properties of electrostatic waves with $B \neq 0$. Wave normal curves for (a) the Langmuir and (b) the upper hybrid branches of the dispersion relation. (c) CMA diagram showing the stop band (hatched) where waves are evanescent. The insets are polar plots of the inverse of the wave normal curves shown in (a) and (b).

quently, the $\omega_{\perp+}$ mode is analogous to the extraordinary mode. As noted by Iwamoto [11], the extraordinary mode is purely transverse in nature. However, the $\omega_{\perp-}$ mode is rather different from the usual extraordinary mode in that the cutoff occurs not at $\omega_L \neq 0$ (see, for example, Ref. [25], pp. 154–156) but at $\omega_-(k=0)=0$ and is asymptotic to $C_s k$ rather than to the upper hybrid frequency. A further point to note is that the low-frequency limit of the biquadratic yields

$$n^2 = 1 + 2\omega_p^2/\Omega_p^2$$

or

$$\omega^2 = \frac{\left(V_A^2/2\right)k^2}{1+\left(V_A^2/2\right)/c^2}. \tag{23}$$

It has been assumed, for simplicity, that $C_s^2/c^2 \ll 1$ and the factor 2 appears because we have defined $V_A^2 \equiv 4\pi mN/B_0^2$ rather than using $V_A^2 = 4\pi m2N/B_0^2$. Expression (23) is simply the cold magnetosonic dispersion relation for waves propagating across the applied magnetic field.

For parallel propagation, (19) reduces to

$$\left(\omega^2 - C_s^2k^2\right)\left[\omega^4 - \left(2\omega_p^2 + \Omega_p^2 + c^2k^2\right)\omega^2 + \Omega_p^2c^2k^2\right] = 0, \tag{24}$$

which can be expressed as

$$\left(\omega^2 - C_s^2k^2\right)\left(\omega^2 - \omega_{\parallel+}^2\right)\left(\omega^2 - \omega_{\parallel-}^2\right) = 0, \tag{25}$$

where we have introduced

$$2\omega_{\parallel\pm}^2 = c^2k^2 + \Omega_h^2 \pm \sqrt{(c^2k^2 + 2\omega_p^2 - \Omega_p^2)^2 + 8\omega_p^2\Omega_p^2}. \tag{26}$$

The similarities between the parallel (22) and perpendicular (26) results are apparent. For $k=0$, we have $\omega^2 = 0, \Omega_h^2$ and as $k \to \infty$, ω is asymptotic to either ck or Ω_p. The usual L and R modes are indistinguishable in an e^+e^- plasma and the $\omega_{\parallel-}$ corresponds to the electron cyclotron mode. However, the absence of a point of inflection on the electron-cyclotron curve indicates that a whistler mode does not exist, as noted by Iwamoto [11] and Stewart and Laing [12]. By considering the low-frequency limit of (24), we find that

$$\omega^2 = \frac{\left(V_A^2/2\right)k^2}{1+\left(V_A^2/2\right)/c^2}, \tag{27}$$

which is now the dispersion relation for Alfvén waves propagating parallel to an applied magnetic field in an e^+e^- plasma. Equation (19) is plotted on Fig. 6(a) for various values of θ between 0 and $\pi/2$.

Now turning to Eq. (20), we find that for perpendicular propagation this equation reduces to

$$\omega^2\left(\omega^2 - c^2k^2 - 2\omega_p^2\right)\left(\omega^2 - C_s^2k^2 - 2\omega_p^2 - \Omega_p^2\right) = 0, \tag{28}$$

or

$$\omega^2 = 0, \qquad \omega^2 = c^2k^2 + 2\omega_p^2, \qquad \omega^2 = C_s^2k^2 + 2\omega_p^2 + \Omega_p^2,$$

and we see that (28) effectively admits an ordinary wave and an upper hybrid wave.

For parallel propagation, Eq. (20) reduces to

$$\omega^2\left(\omega^2 - c^2k^2 - 2\omega_p^2\right)\left(\omega^2 - C_s^2k^2 - \Omega_h^2\right)$$

$$+\Omega_p^2C_s^2k^2\left(\omega^2 - c^2k^2 - 2\omega_p^2c^2/C_s^2\right) = 0. \tag{29}$$

For $k=0$, this equation gives $\omega = 0, \sqrt{2}\omega_p, \Omega_h$, while for $k \to \infty$, $\omega^2 \to \Omega_p^2, c^2k^2, C_s^2k^2$. Equation (20) is plotted in Fig. 6(b) for various values of θ between 0 and $\pi/2$ and the asymptotes derived above for $k \to \infty$ are apparent. Figures 6 are to be contrasted with standard dispersion relation plots for electron-ion plasmas (e.g., [25]).

It is useful to collate the parallel and perpendicular wave modes in a table as before (Table II). Clearly, a simple one-to-one correspondence does not exist, but analogs can generally be drawn between e^+e^- modes and those found in an electron-ion plasma. However, the mode admitted by the dispersion relation (29) asymptotic to $C_s k$ does not admit an obvious correspondence.

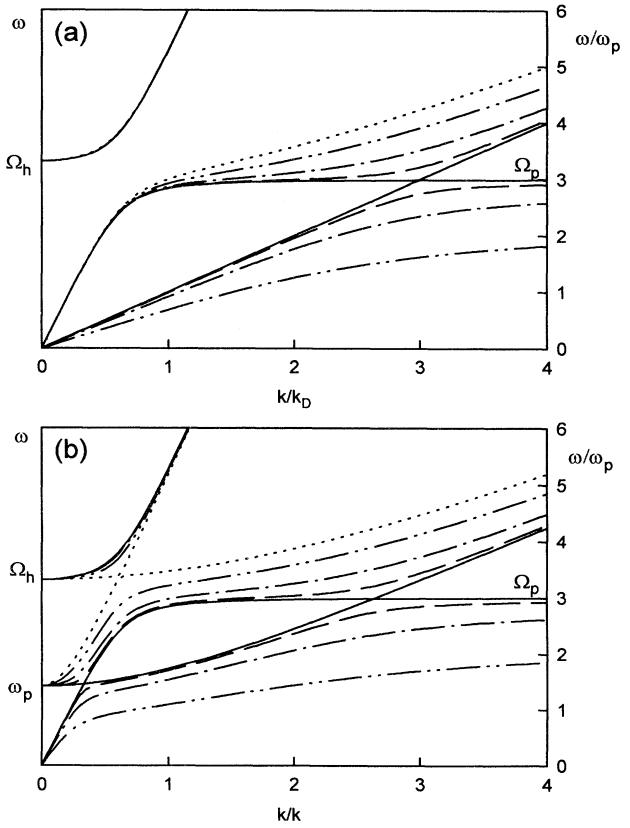

FIG. 6. Dispersion relation for electromagnetic waves with $B \neq 0$. Here (a) corresponds to Eq. (19) and (b) to Eq. (20). Solid lines, $\theta = 0$; dashed lines, $\theta = \pi/20$; chain curve, $\theta = \pi/8$; double chain curve $\theta = \pi/4$; dotted line, $\theta = \pi/2$.

TABLE II. Summary of electromagnetic plasma modes. An asterisk (*) denotes a solution to Eq. (29).

$\theta = 0$		$\theta = \pi/2$	
Dispersion relation	Identification	Dispersion relation	Identification
$\omega^2 = C_s^2 k^2$	acoustic	$\omega = 0$	nonpropagating
$\omega = \omega_{\parallel +}$	R/L mode	$\omega = \omega_{\perp +}$	extraordinary
$\omega = \omega_{\parallel -}$	cyclotron	$\omega = \omega_{\perp -}$	magnetosonic
$\omega = \omega_1{}^*$	electron/cyclotron	$\omega = 0$	nonpropagating
$\omega = \omega_2{}^*$		$\omega^2 = c^2k^2 + 2\omega_p^2$	ordinary wave
$\omega = \omega_3{}^*$	R/L mode	$\omega^2 = C_s^2 k^2 + \Omega_h^2$	upper hybrid wave

To investigate the properties of waves in an e^+e^- plasma further and to derive the appropriate CMA diagrams, we need to rewrite the dispersion relations (19) and (20) in terms of the refractive index

$$\mathbf{n} = c\mathbf{k}/\omega.$$

(Note the definition here differs from that of Sec. III B.) To simplify the analysis further, we make the reasonable assumption that $C_s^2/c^2 \ll 1$. We then obtain

$$n^2 = 1 - \frac{2\omega_p^2/\omega^2}{1 - \Omega_p^2/\omega^2} = 1 - \frac{X}{1 - Y^2}, \tag{30}$$

$$n^2 = \frac{(1 - 2\omega_p^2/\omega^2)(1 - 2\omega_p^2/\omega^2 - \Omega_p^2/\omega^2)}{1 - 2\omega_p^2/\omega^2 - \Omega_p^2/\omega^2 + 2\omega_p^2\Omega_p^2/\omega^4 \cos^2\theta} = \frac{(1 - X)(1 - X - Y^2)}{1 - X - Y^2 + XY\cos^2\theta}. \tag{31}$$

Observe that in the low-frequency limit, (30) reduces to

$$n^2 = 1 + 2\omega_p^2/\Omega_p^2 = 1 + 2c^2/V_A^2,$$

i.e., to (27).

Equation (30) admits resonances at $\omega = \pm\Omega_p$ while cutoffs are found, from $n^2 = 0$, at $\omega = \pm\Omega_h$. A plot of the refractive index surface as a function of ω is given in Fig. 7, illustrating that wave propagation for frequencies satisfying $\Omega_p \le \omega \le \Omega_h$ is evanescent, at least for those modes governed by Eq. (30). The CMA diagram appropriate to this case is shown in Fig. 8 where we have superimposed the wave normal surfaces corresponding to each parameter regime. The evanescent regime $Y < 1$ and $1 - X < Y^2$ in the CMA diagram is simply that found above.

The second factor, Eq. (31), admits much more complicated wave behavior. Resonances are defined at

$$2\omega_\pm^2 = \Omega_h^2 \pm \sqrt{\left(2\omega_p^2 - \Omega_p^2\right)^2 + 8\omega_p^2\Omega_p^2 \sin^2\theta}, \tag{32}$$

which, for $\theta = 0$ implies resonances at $\omega_\pm = \sqrt{2}\omega_p$, Ω_p whereas $\theta = \pi/2$ implies $\omega_\pm = 0, \Omega_h$ (cf. $\omega_{\perp\pm}$). The resonances are found in the frequency ranges $0 \le \omega_- \le \sqrt{2}\omega_p$ and $\Omega_p \le \omega_+ \le \Omega_h$, from which we determine the refractive curves illustrated in Fig. 9. Note the resemblance of these curves to the well-known plot of $n^2(\omega)$ for the extraordinary wave (e.g., Swanson [26], p. 35) although in the limit of $\theta = \pi/2$, the lowest-frequency mode is absent

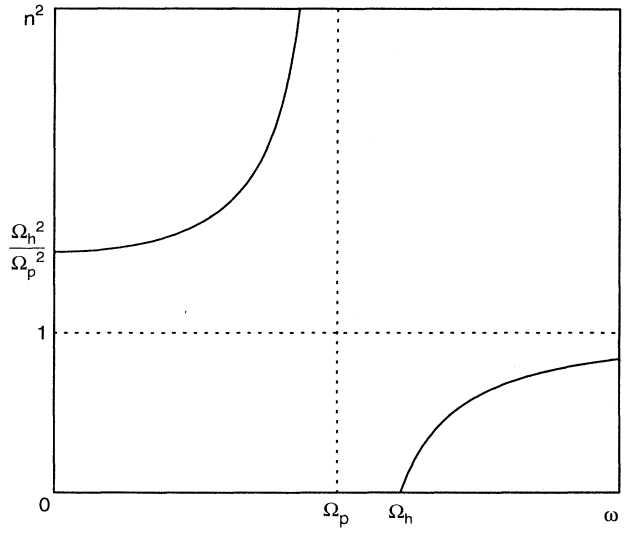

FIG. 7. Refractive index curves for electromagnetic waves.

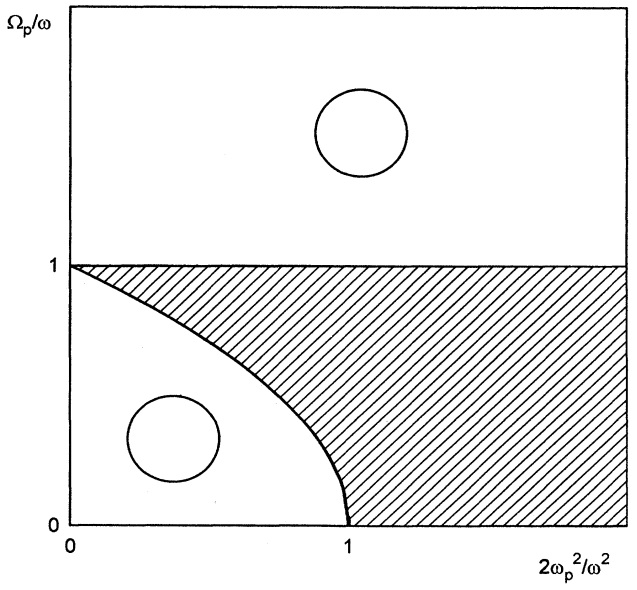

FIG. 8. CMA diagram for electromagnetic waves with $B \neq 0$ [corresponding to Eq. (30)].

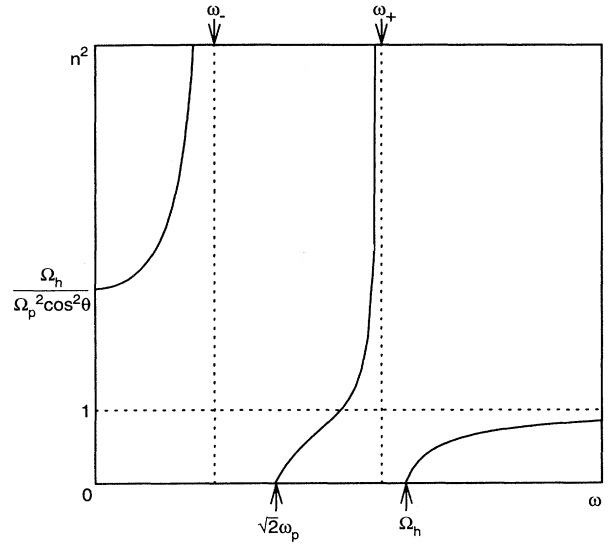

FIG. 9. Refractive index curves for electromagnetic waves.

in the case of the e^+e^- plasma. Waves are evanescent in the frequency ranges $\omega_- < \omega < \sqrt{2}\omega_p$ and $\omega_+ < \omega < \Omega_h$, the latter being similar to the stop band associated with Fig. 8. The CMA diagram for these wave modes is shown in Fig. 10. Clearly, the curve defined by

$$X = \frac{1 - Y^2}{1 - Y^2 \cos^2\theta}$$

defines a resonance in the CMA diagram. The hatched regions of Fig. 10 correspond to evanescent regions ($n^2 < 0$) and it is seen that wave propagation is inadmissible for those frequencies ω satisfying any one of the following conditions:

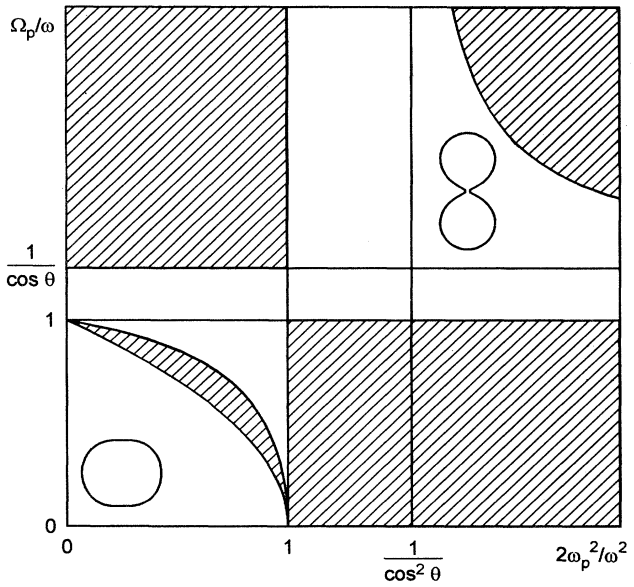

FIG. 10. CMA diagram for electromagnetic waves with $B \neq 0$ [corresponding to Eq. (31)].

$$\Omega_p < \omega < \sqrt{2}\omega_p, \tag{33}$$

$$\sqrt{2}\omega_p < \omega < \Omega_p \cos\theta, \tag{34}$$

$$\omega_- < \omega < \Omega_h, \tag{35}$$

$$\omega < \Omega_p \cos\theta \text{ and } \omega < \omega_+. \tag{36}$$

It is important to remember that, although Fig. 10 indicates that a large region of frequency parameter space does not support wave propagation, this applies only to the factored dispersion relation (31). On using both Figs. 8 and 10 together, we see that the only regimes completely inaccessible to waves are (33) and (35) of the list above.

IV. THE TWO-STREAM INSTABILITY

Consider now two unbounded, uniform interpenetrating streams of electrons and positrons. This models, for example, an electron beam passing through a positron plasma confined in a Penning trap. In the absence of an applied magnetic field, the linearized e^+e^- equations can be combined as

$$\left(\frac{D_1^2}{Dt^2} - C_s^2\nabla^2 + \omega_{p_e}^2\right)\left(\frac{D_2^2}{Dt^2} - C_s^2\nabla^2 + \omega_{p_p}^2\right) n_p = \omega_{p_e}^2\omega_{p_p}^2 n_p, \tag{37}$$

where $D_1/Dt \equiv \partial_t + \mathbf{U}_{1,2}\cdot\nabla$ with $\mathbf{U}_{1,2} \equiv$ the streaming velocity of the electrons and positrons, respectively, and $\omega_{p_{p,e}}^2 \equiv 4\pi e^2 N_{e,p}/m$. For the present, we do not assume equal densities for the electrons and positrons, although equal temperatures are again assumed. The dispersion relation is then

$$\left(\omega_1'^2 - C_s^2k^2 - \omega_{p_e}^2\right)\left(\omega_2'^2 - C_s^2k^2 - \omega_{p_p}^2\right) = \omega_{p_e}^2\omega_{p_p}^2, \tag{38}$$

($\omega_{1,2}' \equiv \omega - \mathbf{U}_{1,2}\cdot\mathbf{k}$) which can be rewritten in the classical form

$$1 = \frac{\omega_{p_e}^2}{\omega_1'^2 - \mathbf{U}_1\cdot\mathbf{k}} + \frac{\omega_{p_p}^2}{\omega_2'^2 - \mathbf{U}_2\cdot\mathbf{k}}. \tag{39}$$

We investigate two cases, (i) the cold limit with $N_e \neq N_p$, and (ii) the warm plasma case with $N_e = N_p = N$.

A. The cold fluid limit

The analysis in this case is entirely standard. Define

$$F(\omega,\mathbf{k}) \equiv \frac{\omega_{p_e}^2}{(\omega - \mathbf{U}_1\cdot\mathbf{k})^2} + \frac{\omega_{p_p}^2}{(\omega - \mathbf{U}_2\cdot\mathbf{k})^2} = 1, \tag{40}$$

and, without loss of generality, suppose $\mathbf{U}_1\cdot\mathbf{k} > \mathbf{U}_2\cdot\mathbf{k}$. The condition for instability is then simply given by

$$|(\mathbf{U}_1 - \mathbf{U}_2)\cdot\mathbf{k}| < \left[1 + \left(\frac{N_p}{N_e}\right)^{1/3}\right]^{3/2}\omega_{p_e}. \tag{41}$$

B. Warm plasma case

We turn now to the warm case and, supposing $N_e = N_p = N$, consider the interesting case of wave propagation such that $\mathbf{U}_{1,2} \parallel \mathbf{k}$. Let $U_1 > U_2$. The introduction of the phase velocity $V_p \equiv \omega/k$ shows that two cases need be considered. The first corresponds to the case $U_1 - C_s > U_2 + C_s$, and the second to $U_1 - U_2 < 2C_s$. Thus, as is well known, the two-stream instability is quenched when the relative streaming satisfies $U_1 - U_2 < 2C_s$. To determine the most unstable wave number k and the maximum growth rate, rewrite (39) as

$$\omega'^4 - 2\left[\left(V^2 + C_s^2\right)k^2 + \omega_p^2\right]\omega'^2 + \left(V^2 - C_s^2\right)k^2\left[\left(V^2 - C_s^2\right)k^2 - 2\omega_p^2\right] = 0, \quad (42)$$

where $\omega' \equiv \omega - Uk$, $U \equiv (U_1 + U_2)/2$ and $V \equiv (U_1 - U_2)/2$. It is evident that to have a zero of (42) for which $\omega'^2 < 0$, we require positive values of k to satisfy

$$k^2 < \frac{8\omega_p^2}{(U_1 - U_2)^2 - 4C_s^2}. \quad (43)$$

The condition for such k values to exist can also be derived graphically, viz., $U_1 - U_2 > 2C_s$. Since

$$\omega'^2 = \omega_p^2 + (V^2 + C_s^2)k^2 \pm \omega_p\left[\omega_p^2 + 4(V^2 - C_s^2)k^2\right]^{1/2},$$

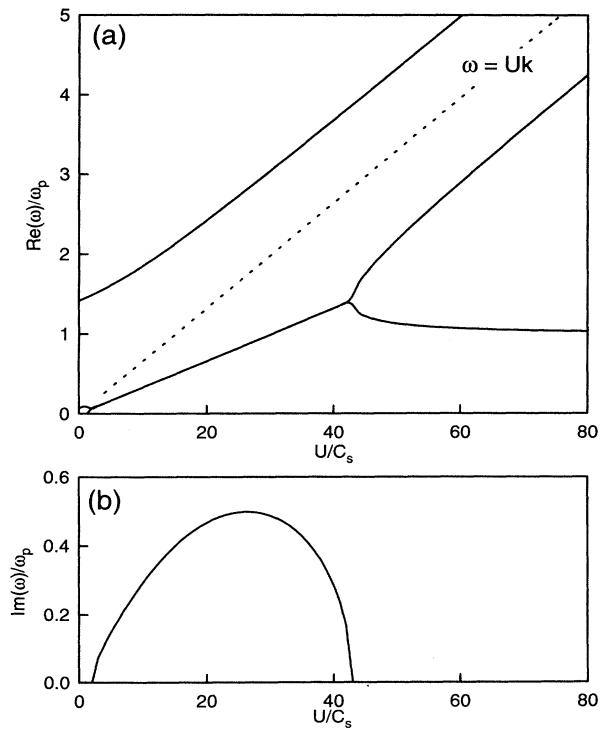

FIG. 11. Dependence of mode frequency on beam velocity for waves in a beam-plasma system, showing the unstable region that occurs when the Langmuir mode of the plasma couples with the Doppler-shifted mode of the beam.

the wave number of the most rapidly growing mode is

$$k^2 = \frac{3}{4}\frac{\omega_p^2}{V^2 - C_s^2}, \quad (44)$$

for which

$$\omega' = \pm\frac{\sqrt{15}}{2}\omega_p, \quad \pm i\frac{\omega_p}{2}, \quad (45)$$

giving a maximum growth rate of $\omega_p/2$. In Fig. 11, we show the real and imaginary part of the mode frequencies for a range of beam energies.

These results are similar to the usual two-stream instability in an electron-ion plasma except that the factor $(m_e/m_i)^{1/3}$ (where m_i is the ion mass) multiplying the growth rate is unity for the e^+e^- case, leading to substantially larger growth, as first pointed out by Tsytovich and Wharton [10].

V. SOLITARY WAVES

Low-frequency ion-acoustic waves can propagate as solitary waves in an ion-electron plasma. The situation for an e^+e^- plasma is complicated by the presence of equal-mass species, which prevents one from approximating the electrons by an isothermal Boltzmann distribution $n_e = n_0 \exp[e\phi/\kappa T]$, where ϕ denotes the electrostatic potential [27]. Consider the two-fluid equations in the absence of a magnetic field and introduce the following normalizations (based on the Debye length $\lambda_D^2 = \gamma\kappa T/4\pi N e^2$), where $N = N_e = N_p$ is the undisturbed equilibrium number density. Then, using

$$\bar{x} = \frac{x}{\lambda_D}, \quad \bar{t} = \frac{tC_s}{\lambda_D}, \quad \bar{\mathbf{u}}_j = \frac{\mathbf{u}_j}{C_s}, \quad \bar{n}_j = \frac{n_j}{N}, \quad \bar{\phi} = \frac{e\phi}{\gamma\kappa T},$$

yields the normalized one-dimensional (1D) equations

$$\frac{\partial n_j}{\partial t} + \frac{\partial}{\partial x}(n_j u_j) = 0,$$
$$m n_j\left(\frac{\partial u_j}{\partial t} + u_e\frac{\partial u_e}{\partial x}\right) = -\frac{\partial p_j}{\partial x} + q n_j E, \quad (46)$$
$$\frac{\partial^2\phi}{\partial x^2} = 4\pi e(n_e - n_p),$$

where, for convenience, the bars have been dropped. We introduce the comoving Mach number M of the propagating disturbance such that $\xi = \bar{x} - M\bar{t}$. On seeking stationary structures subject to the usual boundary conditions $n_p(\pm\infty) = n_e(\pm\infty) = 1$, $u_p(\pm\infty) = u_e(\pm\infty) = 0$ and $\phi(\pm\infty) = 0$, we obtain

$$\frac{d}{d\xi}\left(\frac{M^2}{n_e} + n_e\right) = n_e\frac{d\phi}{d\xi},$$
$$\frac{d}{d\xi}\left(\frac{M^2}{n_p} + n_p\right) = -n_p\frac{d\phi}{d\xi}, \quad (47)$$
$$\frac{d^2\phi}{d\xi^2} = n_e - n_p.$$

Equations (47) are integrated easily, yielding

$$\begin{aligned} \ln n_e + \left(\frac{1}{n_e^2} - 1\right)\frac{M^2}{2} &= \phi, \\ \ln n_p + \left(\frac{1}{n_p^2} - 1\right)\frac{M^2}{2} &= -\phi, \\ \frac{d^2\phi}{d\xi^2} &= n_e - n_p, \end{aligned} \tag{48}$$

but this approach, which is exploited in ion-electron plasmas, is not particularly helpful here. Instead, we utilize an approach suggested by Huibin and Kelin [28], which is to expand the plasma variables as a power series in $\mathrm{sech}\mu\xi$, i.e.,

$$\begin{aligned} n_e &= \sum_{i=0}^{\infty} a_i \mathrm{sech}^i \mu\xi, \\ n_p &= \sum_{i=0}^{\infty} b_i \mathrm{sech}^i \mu\xi, \\ \phi &= \sum_{i=0}^{\infty} c_i \mathrm{sech}^i \mu\xi. \end{aligned} \tag{49}$$

By substituting (49) into (47), we obtain the following recursion relations for the coefficients a_i:

$$\left(a_0^2 - M^2\right) a_1 = a_0^3 c_1,$$

$$2a_0 a_1^2 + 2\left(a_0^2 - M^2\right) a_2 = 3a_0^2 a_1 c_1 + 2a_0^3 c_2,$$

$$n\left(a_0^2 - M^2\right) a_n + \sum_{\substack{m+j+\ell=n \\ \ell<n}} a_m a_j \ell a_\ell = n a_0^3 c_n + \sum_{\substack{\ell+m+j+p=n \\ \ell<n}} a_m a_j a_p \ell c_\ell, \tag{50}$$

for the b_i,

$$\left(b_0^2 - M^2\right) b_1 = -b_0^3 c_1,$$

$$2b_0 b_1^2 + 2\left(b_0^2 - M^2\right) b_2 = -3ab_0^2 b_1 c_1 - 2b_0^3 c_2,$$

$$n\left(b_0^2 - M^2\right) b_n + \sum_{\substack{m+j+\ell=n \\ \ell<n}} b_m b_j \ell b_\ell = -n b_0^3 c_n - \sum_{\substack{\ell+m+j+p=n \\ \ell<n}} b_m b_j b_p \ell c_\ell, \tag{51}$$

and for the c_i,

$$\begin{aligned} a_0 &= b_0, \\ \mu^2 c_1 &= a_1 - b_1, \\ 4\mu^2 c_2 &= a_2 - b_2, \\ \mu^2\left[n^2 c_n - (n-1)(n-2)c_{n-2}\right] &= a_n - b_n. \end{aligned} \tag{52}$$

The reason for our expanding in powers of $\mathrm{sech}\mu\xi$ is apparent from the symmetry conditions imposed by the boundary conditions above and, clearly,

$$a_0 = b_0 = 1, \qquad c_0 = 0. \tag{53}$$

From the $O(1)$ recursion relation, we find

$$a_1 = -b_1 = \frac{c_1}{1 - M^2}, \tag{54}$$

which implies that

$$\left(\mu^2 - \frac{2}{1 - M^2}\right) c_1 = 0. \tag{55}$$

To ensure that $c_1 \neq 0$ (otherwise $a_1 = b_1 = 0$, from which all higher order terms in the expansion are identically zero), we require $\mu^2 = 2/(1 - M^2)$ and $\mu^2 > 0$. Thus, a necessary (although not sufficient) condition for the existence of stationary solitary wave structures in an e^+e^- plasma is that they be subsonic with respect to the electron-positron sound speed, i.e., $M = V_p/C_s < 1$, in contrast with electron-ion plasmas where both subsonic and supersonic propagation are possible. The choice of c_1 reflects the imposition of the initial condition that would ordinarily be required to solve (47) and (48) directly. It can be shown that $c_2 = 0$ and that

$$a_2 = \frac{1}{12(1 - M^2)}(1 - 18M^2),$$

$$b_2 = \frac{1}{2(1 - M^2)}\left(17/6 - 3M^2\right),$$

and in general, for $n > 2$,

$$\begin{aligned} a_n &= \frac{\displaystyle\sum_{\substack{\ell+m+j+p=n \\ \ell<n}} a_m a_j a_p \ell c_\ell - \sum_{\substack{\ell+m+j=n \\ \ell<n}} a_m a_j \ell a_\ell}{n\left(1 - M^2\right)} + \frac{c_n}{1 - M^2}, \\ b_n &= -\frac{\displaystyle\sum_{\substack{\ell+m+j+p=n \\ \ell<n}} b_m b_j b_p \ell c_\ell - \sum_{\substack{\ell+m+j=n \\ \ell<n}} b_m b_j \ell b_\ell}{n\left(1 - M^2\right)} + \frac{c_n}{1 - M^2}, \\ c_n &= \frac{n-2}{n+1} c_{n-2} + \frac{a_n(1 - M^2)}{2(n^2 - 1)} - \frac{b_n(1 - M^2)}{2(n^2 - 1)}. \end{aligned} \tag{56}$$

These relations can be used to compute solitary wave solutions to (47) recursively. In Fig. 12, examples of different amplitude solitary waves for a Mach number of 0.5 are presented. The smaller the amplitude of the solitary wave, the more closely it is approximated by a leading order $\mathrm{sech}\mu\xi$ or a $\mathrm{sech}^2\mu\xi$ solution. We find numerically that $\bar{\phi} = e\phi/\gamma\kappa T$ has a maximum amplitude of ~ 0.2. The effect of varying the Mach number of the solitary wave is illustrated in Fig. 13. The wider pulse corresponds to a wave propagating with a Mach number

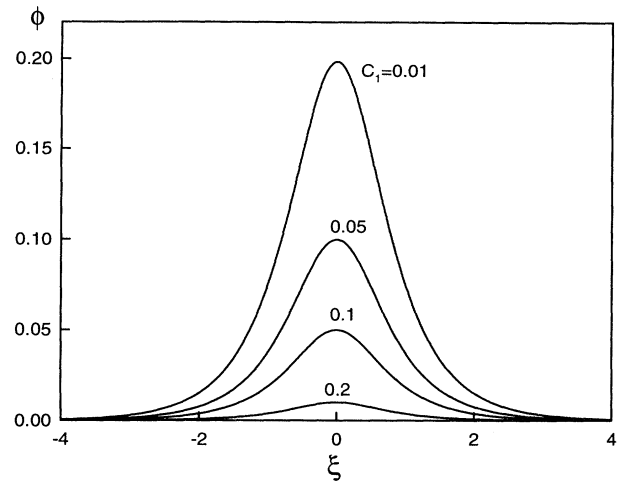

FIG. 12. Examples of solitary waves of different amplitudes which correspond to a Mach number of 0.5.

$M = 0.2$ whereas increasing M to $M = 0.8$ narrows the pulse significantly, although the amplitude is unchanged. These properties distinguish solitary waves in an e^+e^- plasma from those found in a conventional ion-electron plasma.

Berezhiani *et al.* have investigated solitary waves in relativistic plasmas [4]. Their treatment is quite unlike ours in that they assume the plasma to be cold. Consequently, acoustic modes are absent in their analysis and they focus exclusively on magnetic effects. The appropriate analog of our results are the well-known ion-acoustic solitary waves that can exist in an ion-electron plasma (Refs. [27] and [28]).

VI. CONCLUSIONS

Linear and nonlinear collective modes in a nonrelativistic electron-positron plasma have been investigated on the basis of a simple two-fluid model. This problem is particularly timely in view of recent progress made in the production of pure positron plasmas in the laboratory. Thus, laboratory experiments on electron-positron plasmas are already under consideration. Among the experiments that could be undertaken are instabilities in the beam-plasma system, studies of Faraday rotation where one could change continuously from left to right hand polarization by changing from a pure electron plasma through a neutralized electron-positron plasma to a pure positron plasma. The nonlinear properties of electron-positron plasmas are a potentially rich field of study. Solitary wave structures in the beam-plasma system are now experimentally accessible. Transport studies are also of interest: The electron-positron plasma in a magnetic field is unique in that both species are equally and strongly magnetized.

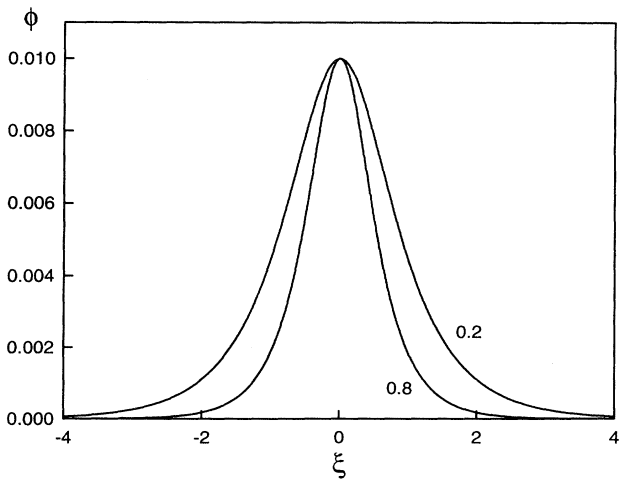

FIG. 13. Examples showing the variation of solitary wave structure with Mach number $M = 0.2$ and 0.8.

Another approach to the study of e^+e^- plasmas is the use of numerical simulations. These techniques have already been applied to relativistic e^+e^- plasmas. For example, Gallant *et al.* used a 1D particle-in-cell simulation to investigate relativistic perpendicular shocks in e^+e^- plasmas. They found e-mode radiation and discussed their results in relation to observed centimeter wave emission from compact extragalactic radio sources. Recently, Zhao *et al.* [29,30] have used a 3D fully electromagnetic and relativistic particle-in-cell code to explore nonlinear Alfvén waves and particle acceleration in the relativistic electron-positron beam-plasma system. Such techniques could also be applied to nonrelativistic e^+e^- plasmas. A problem that is of current interest is the study of the beam-plasma system and, in particular, the growth and saturation of instabilities and processes that lead to plasma heating. Other problems of interest are the nonlinear phenomena where e^+e^- plasmas differ most from electron-ion plasmas. These include solitary wave structures in stationary plasmas and in the beam-plasma system, cross-field transport, and the phenomena of holes and clumps [31].

In this paper, we have exploited the equal-mass character of e^+e^- plasmas to considerably simplify the linear mode analysis. Many of the phenomena found in conventional electron-ion plasmas exist in modified form, while others, notably the whistler wave, the lower hybrid wave and Faraday rotation, are absent. As the simplest extension to a nonhomogeneous plasma, we have discussed the two-stream instability, finding that it is similar to the electron-ion case, except that the effective growth rate is considerably larger because the ratio m_e/m_i is unity.

The nonlinear analysis, on the other hand, is complicated by the equal-mass character of the plasma and requires an approach rather different from that used conventionally in an electron-ion plasma. For solitary wave structures, some interesting differences from the electron-ion case emerge. Notably, only subsonic solutions are found to exist, while the pulse width, rather than its amplitude, is related to the wave speed.

Clearly, this paper only hints at much of the intriguing plasma physics yet to be discovered in equal-mass plasmas and planned experiments could provide many surprises.

ACKNOWLEDGMENTS

We thank M. D. Tinkle and C. M. Surko for valuable comments on the manuscript. G.P.Z. acknowledges the partial support of a National Science Foundation Young Investigator Grant No. ATM-9357861. The work at the University of California, San Diego is supported by the Office of Naval Research.

[1] C. M. Surko, M. Leventhal, and A. Passner, Phys. Rev. Lett. **62**, 901 (1989).
[2] C. M. Surko and T. J. Murphy, Phys. Fluids B **2**, 1372 (1990).
[3] R. G. Greaves, M. D. Tinkle, and C. M. Surko, Phys. Plasmas **1**, 1439 (1994).
[4] V. I. Berezhiani, V. Skarka, and S. Mahajan, Phys. Rev. E **48**, 3252 (1993).
[5] U. A. Mofiz and A. A. Mamun, Phys. Fluids B **5**, 1667 (1993).
[6] Y. A. Gallant *et al.*, Astrophys. J. **391**, 73 (1992).
[7] L. N. Tsintsadze, Astrophys. Space Sci. **191**, 151 (1992).
[8] U. A. Mofiz, Phys. Rev. A **40**, 2203 (1989).
[9] N. Iwamoto, Phys. Rev. A **39**, 4076 (1989).
[10] V. Tsytovich and C. B. Wharton, Comments Plasma Phys. Controlled Fusion **4**, 91 (1978).
[11] N. Iwamoto, Phys. Rev. E **47**, 604 (1993).
[12] G. A. Stewart and E. W. Laing, J. Plasma Phys. **47**, 295 (1992).
[13] G. A. Stewart, J. Plasma Phys. **50**, 521 (1993).
[14] S. Y. Abdul-Rassak and E. W. Laing, J. Plasma Phys. **50**, 125 (1993).
[15] G. Gibson, W. C. Jordan, and E. J. Lauer, Phys. Rev. Lett. **5**, 141 (1960).
[16] G. Gibson, W. C. Jordan, and E. J. Lauer, Phys. Fluids **6**, 116 (1963).
[17] H. Boehmer, in *Slow Positron Beam Techniques for Solids and Surfaces,* edited by E. Ottewitte and A. Weiss, AIP Conf. Proc. No. 303 (AIP, New York, 1994), p. 422.
[18] T. E. Cowan *et al.*, Hyperfine Interactions **76**, 135 (1993).
[19] A. Mohri *et al.*, *Elementary Processes in Dense Plasmas* (Addison-Wesley, Reading, MA, in press).
[20] J. P. Schermann and F. G. Major, Appl. Phys. **16**, 225 (1978).
[21] R. G. Greaves, M. D. Tinkle, and C. M. Surko, *Nonneutral Plasmas II* (AIP, New York, in press).
[22] R. W. Bussard, R. Ramaty, and R. J. Drachman, Astrophys. J. **228**, 928 (1979).
[23] N. Guessoum, R. Ramaty, and R. E. Lingenfelter, Astrophys. J. **378**, 170 (1991).
[24] P. C. Clemmow and J. P. Dougherty, *Electrodynamics of Particles and Plasmas* (Addison-Wesley, Redwood City, CA, 1990).
[25] D. R. Nicholson, *Introduction to Plasma Theory* (Wiley, New York, 1983).
[26] D. G. Swanson, *Plasma Waves* (Academic Press, Boston, 1989).
[27] G. P. Zank and J. F. McKenzie, J. Plasma Phys. **39**, 183 (1988).
[28] L. Huibin and W. Kelin, J. Plasma Phys. **44**, 151 (1990).
[29] J. Zhao, J. I. Sakai, K.-I. Nishikawa, and T. Neubert, Phys. Plasmas **1**, 4114 (1994).
[30] J. Zhao, K. I. Nishikawa, J. I. Sakai, and T. Neubert, Phys. Plasmas **1**, 103 (1994).
[31] R. H. Berman, D. J. Tetreault, and T. H. Dupree, Phys. Fluids **28**, 155 (1985).